Analysis of the kinetic energy from fission fragments using dynamical model

S. Takagi[1,2,*], *Y.* Aritomo[1], *K.* Hirose[2], and *K.* Nishio[2]

[1]Graduate School of Science and Engineering, Kindai University, Higashi-Osaka, Osaka 577–8502, Japan
[2]Advanced Science Research Center, Japan Atomic Energy Agency, Tokai, Ibaraki 319–1195, Japan

Abstract. It is known that the kinetic energy of individual fragments for fission of actinides is constant at about 100 MeV for light fragments and that for heavy fragments decreases with mass number. The kinetic energy is, for example, important for evaluating the prompt-neutron spectrum in the laboratory system. However, its theoretical study has not been attempted in detail so far. We have calculated them in thermal-neutron induced fission of ^{235}U using the dynamical model, considering the Coulomb energy at the scission point and the pre-scission kinetic energy. The calculated results reproduce the experimental data. It is found that the pre-scission kinetic energy has about 5% contribution in the kinetic energy.

1 Introduction

There are several fission observables such as fission fragment mass distribution (FFMD), total kinetic energy (TKE), and number of emitted neutrons for each fragment. In the framework of the classical liquid drop model, the saddle point and fission valley are located at mass-symmetry, thus the FFMD is predicted to have a mass-symmetric shape. By introducing the shell correction energy [1, 2], the actinide nucleus splits into mass asymmetry, explaining the experimental data. For a wide range of actinide nuclides, the average mass number of the heavy fragments is known to be constant at about $A = 140$ [3, 4]. Proton shell of $Z = 54$ is argued to have an important role to determine the degree of mass-asymmetry [5], which is theoretically explained in [6]. The total kinetic energy mostly originates from the Coulomb energy at the scission point. Neutron multiplicity, which reflects the deformation of the fragment at the scission point, is known to have a sawtooth structure as a function of the fission fragment mass.

Here, we focused on the kinetic energy of individual fission fragments. In actinide nuclides from thorium to californium, the average kinetic energy of light fragments is known to be constant with values from 99 MeV to 107 MeV, depending on the nuclide, whereas for heavy fragments it tends to decrease nearly linearly with mass number [7–19]. These trends have not been theoretically studied so far. Although Coulomb energy at the scission point is the dominant origin for kinetic energy, the pre-scission kinetic energy (PKE) may also contribute. Among the various theoretical models, the scission point model, for example, cannot introduce PKE because the calculation is performed to configure the shape at the scission point [20, 21]. On the other hand, the dynamical models such as the Langevin approach can evaluate the time evolution of nuclear shape, thus can define PKE for each fragment [22, 23]. We calculated the individual kinetic energy by taking into account the PKE for thermal-neutron induced fission of ^{235}U, ^{235}U$(n_{\rm th}, f)$, in the Langevin framework. The calculation results show that the kinetic energy of the individual fragments reproduces the experimental trend as well as FFMD and TKE.

2 Model

We use the three-dimensional Langevin equation to calculate the time evolution of nuclear shape. The nuclear shape is defined by the two-center parametrization [24], with three shape parameters, z, δ, and α.

$$\begin{aligned} z &= \frac{z_0}{BR}, \qquad \delta = \frac{3(a-b)}{2a+b}, \quad \alpha = \frac{A_1 - A_2}{A_{CN}}, \\ B &= \frac{3+\delta}{3-2\delta}, \quad R = r_0 {A_{CN}}^{1/3}, \quad r_0 = 1.2\,[\mathrm{fm}]. \end{aligned} \tag{1}$$

The symbol z corresponds to the distance between the center of two potentials, δ denotes the deformation parameter of each fragment ($\delta = \delta_1 = \delta_2$), and α is the mass asymmetry of fragments. These three collective coordinates are abbreviated as q, with $q = \{z, \delta, \alpha\}$. a and b represent the half-length of the ellipse axes in the z_0 and ρ (z_0 and ρ are the cylinder coordinates of the model). A_{CN} is the mass number of the compound nucleus $A_{CN} = A_1 + A_2$, represented by the fragment mass A_1 and A_2. R indicates the radius of the spherical compound nucleus.

The potential energy is a sum of the liquid drop (LDM) and microscopic (SH) parts.

$$\begin{aligned} V(q,T) &= V_{\rm LDM}(q) + V_{\rm SH}(q,T), \\ V_{\rm SH}(q,T) &= E^0_{\rm SH}(q)\Phi(T), \\ E^0_{\rm SH}(q) &= \Delta E_{\rm shell}(q) + \Delta E_{\rm pair}(q), \\ \Phi(T) &= \exp\left(-\frac{aT^2}{E_d}\right). \end{aligned} \tag{2}$$

*e-mail: shinya_takagi@kindai.ac.jp

In Eq. (2), the $V_{\rm LDM}$ is the potential from the finite-range liquid drop model [25]. The microscopic potential $V_{\rm SH}$ at $T = 0$ is calculated as a sum of the shell correction energy $\Delta E_{\rm shell}(q)$, evaluated by the Strutinsky method [1, 2], and the pairing correction energy $\Delta E_{\rm pair}(q)$ [26]. T is the temperature of nucleus and a is the level density parameter. The shell damping energy $E_{\rm d}$ is chosen as 20 MeV given by Ignatyuk *et al.* [27].

The Langevin equation [28] is given as

$$\begin{aligned}\frac{{\rm d}q_i}{{\rm d}t} &= \left(m^{-1}\right)_{ij} p_j, \\ \frac{{\rm d}p_i}{{\rm d}t} &= -\frac{\partial V}{\partial q_i} - \frac{1}{2}\frac{\partial}{\partial q_i}(m^{-1})_{jk} p_j p_k \\ &\quad - \gamma_{ij}(m^{-1})_{jk} p_k + g_{ij} R_j(t),\end{aligned} \tag{3}$$

where $q_i = \{z, \delta, \alpha\}$ and $p_i = m_{ij}\frac{{\rm d}q_j}{{\rm d}t}$ denotes the momentum conjugated to q_i. In Eq. (3), m_{ij} and γ_{ij} are the shape-dependent collective inertia and friction tensors. We adopted the hydrodynamical inertia tensor m_{ij} in the Werner-Wheeler approximation [29]. The one-body friction tensor γ_{ij} is calculated in the wall-and-window formula [30].

The total kinetic energy of the fission fragments can be expressed as a sum of the total Coulomb energy at the scission point $V_{\rm Coul}$ (TCE) and pre-scission total kinetic energy of both fragments $E_{\rm pre}$ (PKE).

$$\begin{aligned}{\rm TKE} &= V_{\rm Coul} + E_{\rm pre}, &(4)\\ &= \frac{Z_1 Z_2 e^2}{D} + \frac{1}{2}(m^{-1})_{ij} p_i p_j &(5)\end{aligned}$$

Z_1 and Z_2 are the nuclear charge of fission fragments. D is the center-of-mass distance between the fragments at the scission point, defined by the shape that the neck-radius becomes zero. $E_{\rm pre}$ is calculated at the instance of nuclear rupture. Finally, the kinetic energy of each fragment (FKE) is calculated as follows using the momentum conservation law.

$$\begin{aligned}{\rm FKE}_L &= \frac{A_H}{A_L + A_H}{\rm TKE}, &(6)\\ {\rm FKE}_H &= \frac{A_L}{A_L + A_H}{\rm TKE}, &(7)\end{aligned}$$

where A_L and A_H are the mass of light and heavy fragments, respectively.

3 Results

Figure 1 shows (a) FFMD and (b) TKE distribution, Y(TKE), for ^{236}U at the compound-nucleus excitation energy $E^* = 6.54$ MeV in comparison with the experimental data of $^{235}{\rm U}(n_{\rm th}, f)$ [12, 18, 19]. The calculated result of FFMD agrees well with the experimental data in terms of the mass-asymmetry giving the largest yield and the width of light- and heavy-fragment distribution. The calculated Y(TKE) has a peak around 170 MeV as seen in the experimental data. Although the calculated Y(TKE) has a narrower distribution than the measured data, the general trend is demonstrated in the dynamical model.

Figure 2(a) shows the calculated fission events on the fragment mass and TKE. The panel (b) of Fig. 2 is the distribution on the mass vs FKE. The fission Q-value, represented by the mass [31] and the excitation-energy of the compound nucleus is shown in Fig. 2(a). The mass-TKE events distribute around 175 MeV, and the small yield at the symmetric fission at ~ 165 MeV is obtained. The mass-FKE distribution is centered around 103 MeV for the light fragments and decreases with mass number for the heavy fragments. The lower part of Fig. 2 shows the (c) average TKE and (d) average FKE as a function of fragment mass, obtained from the calculation and compared with the experimental data. The average TKE at symmetric fission overestimates the experimental data, and TKE around $A_H = 132$ underestimates the data. Still the region $A_H = 140$ having the most dominant yield is explained in the calculation. For the average FKE, the measured data are reproduced in our calculation. Especially, the constant behavior of the average FKE in the light-fragment region is well reproduced. The correct estimation of D in Eq. (5) is important to reproduce the experimental trend of the FKE.

Figure 3 shows the (a) mass-TCE and (b) mass-PKE plot. The black open circles indicate the average value for each fragment. The mass-TCE distribution shows a similar trend to the mass-TKE in Fig. 2(a). The mass-PKE distribution in (b) is centered around 9 MeV, and no strong dependence on the fragment mass asymmetry is found. It is found that the PKE has a 5% contribution to the TKE value. The lower part of Fig. 3 shows the (c) Coulomb part of each-fragment kinetic energy (FCE) and the (d) pre-scission kinetic energy for each fragment (FPKE). The FCE for light fragments is distributed in the restricted region of 80 MeV to 105 MeV, whereas the heavy fragment ranges widely from 80 MeV at $A_H = 125$ u to 40 MeV at 165 u. The mean value of FPKE decreases linearly through all the fragments with the mass from 6 MeV to 3 MeV.

4 Summary

Kinetic energy of individual fragments has been investigated by the three-dimensional Langevin equation. We studied thermal-neutron induced fission of ^{235}U. The calculated results reasonably reproduce the experimental data, especially the constant values of average kinetic energy for light fragments as well as the linearly decreasing trend with mass in the heavy-fragment region. The contribution of the pre-scission kinetic energy is found to be about 5% of the total kinetic energy.

References

[1] V.M. Strutinsky, Nucl. Phys. A **95**, 420 (1967)
[2] V.M. Strutinsky, Nucl. Phys. A **122**, 1 (1968)
[3] C. Wagemans, ed., *The nuclear Fission process* (CRC Press, 1991)
[4] R. Vandenbosch, J.R. Huizenga, *Nuclear fission* (Academic Press, Inc., New York, 1973)

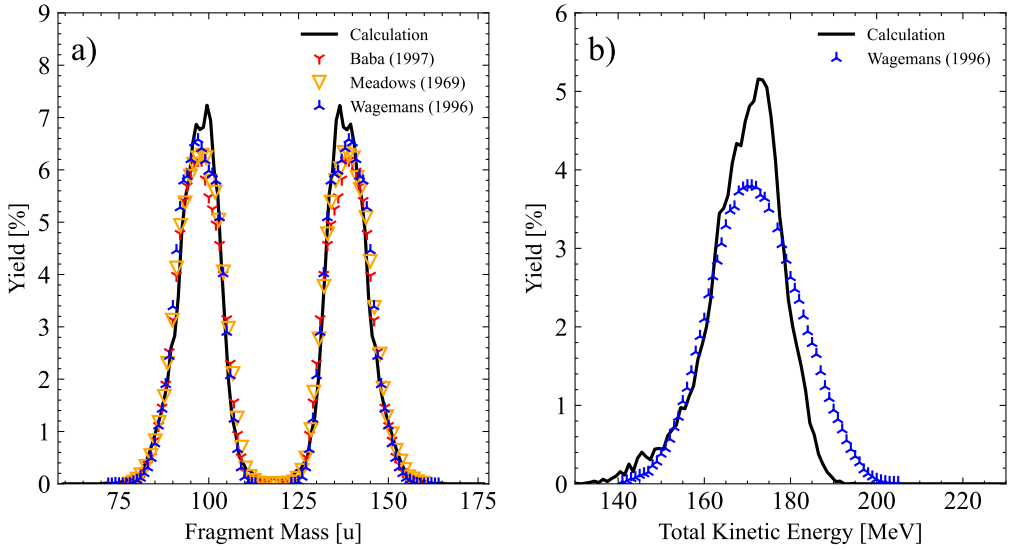

Figure 1: (a) FFMD and (b) TKE distribution for ^{236}U at $E^* = 6.54$ MeV. The calculation results are shown in black lines. The experimental data of ^{235}U($n_{\rm th}$, f) are shown by red, orange, and blue symbols [12, 18, 19].

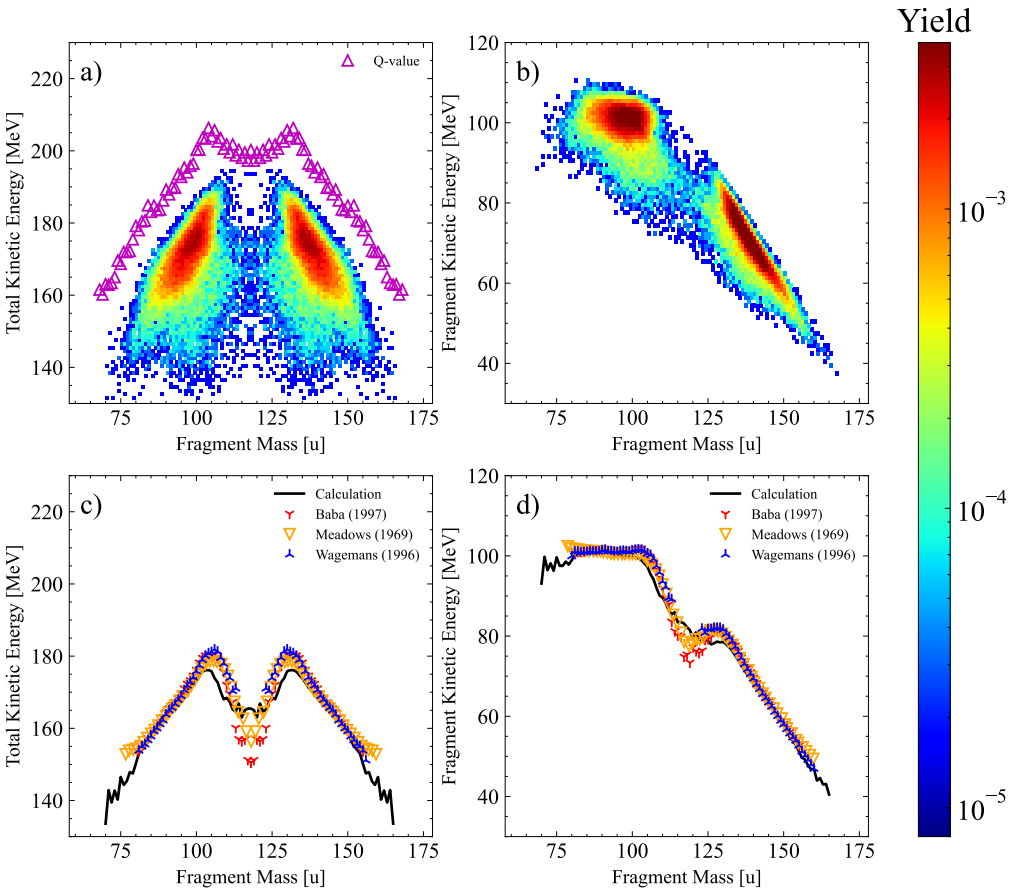

Figure 2: Fission fragment (a) mass-TKE, (b) mass-FKE distributions, (c) average TKE and (d) average FKE distributions as a function of fragment mass for ^{236}U. A purple symbol in (a) is the Q-value. The black lines in (c) and (d) are the results of the present calculations, and the symbols are the experimental data of ^{235}U($n_{\rm th}$, f).

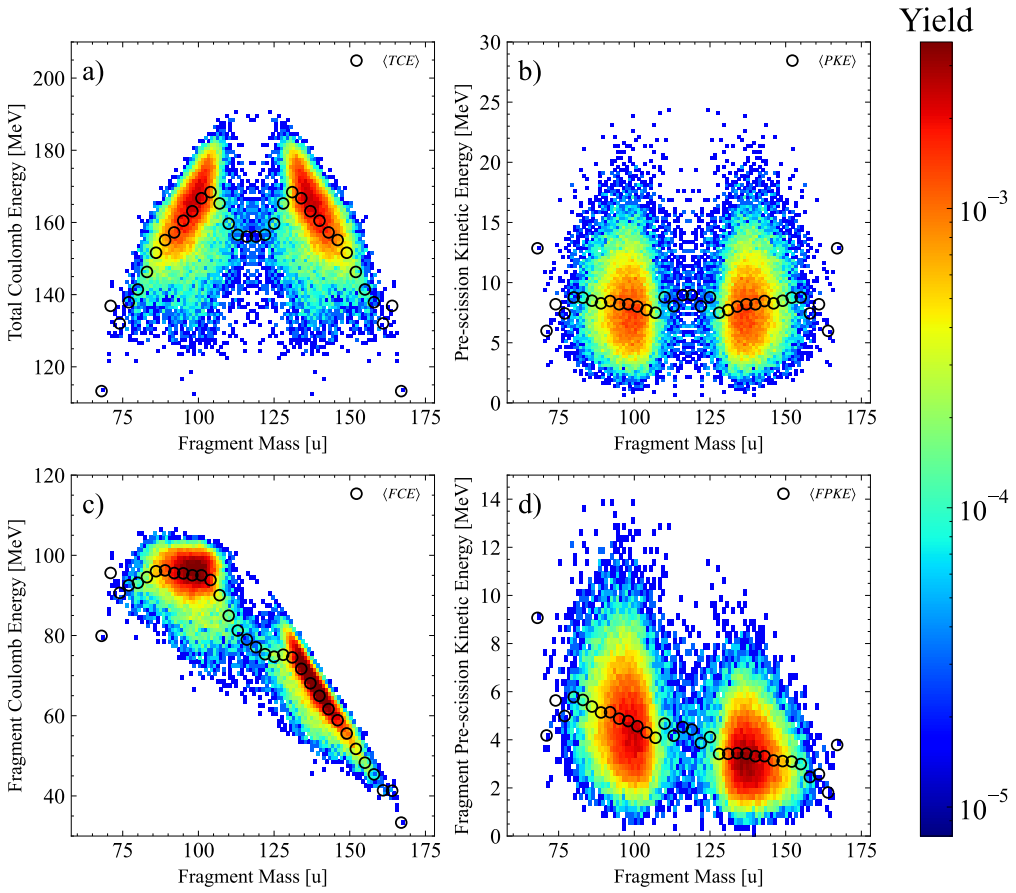

Figure 3: Fission fragment (a) mass-TCE, (b) mass-PKE, (c) mass-FCE, and (b) mass-FPKE distributions for ^{236}U. The averages of each distribution are shown as black open circles.

[5] K.H. Schmidt, J. Benlliure, A.R. Junghans, Nucl. Phys. A **693**, 169 (2001)
[6] G. Scamps, C. Simenel, Nature **564**, 382 (2018)
[7] M. Asghar, P. D'hondt, C. Guet, P. Perrin, C. Wagemans, Phys. Rev. C Nucl. Phys. **292**, 225 (1977)
[8] M. Asghar, F. Caïtucoli, B. Leroux, M. Maurel, P. Perrin, G. Barreau, Nucl. Phys. A **368**, 319 (1981)
[9] M. Asghar, F. Caïtucoli, B. Leroux, M. Maurel, P. Perrin, G. Barreau, Nucl. Phys. A **373**, 225 (1982)
[10] C. Wagemans, E. Allaert, F. Caïtucoli, P. D'hondt, G. Barreau, P. Perrin, Phys. Rev. C Nucl. Phys. **369**, 1 (1981)
[11] C. Wagemans, E. Allaert, A. Deruytter, R. Barthélémy, P. Schillebeeckx, Phys. Rev. C Nucl. Phys. **30**, 218 (1984)
[12] C. Wagemans, L. Demattè, S. Pommé, P. Schillebeeckx, Nucl. Phys. A **597**, 188 (1996)
[13] H. Schmitt, W.E. Kiker, C. Williams, Phys. Rev. **137**, 837 (1965)
[14] H. Schmitt, J.H. Neiler, F.J. Walter, Phys. Rev. (1966)
[15] K. Nishio, Y. Nakagome, I. Kanno, I. Kimura, J. Nucl. Sci. Technol. **32**, 404 (1995)
[16] F. Caïtucoli, C. Wagemans, P. Perrin, E. Allaert, P. D'hondt, M. Asghar, Nucl. Phys. A **369**, 15 (1981)
[17] F. Caïtucoli, M. Asghar, B. Leroux, G. Barreau, K. Hamadache, A. Sicre, T.P. Doan, M. Allab, Nucl. Phys. A **394**, 360 (1983)
[18] J.W. Meadows, Phys. Rev. **177**, 1817 (1969)
[19] H. Baba, T. Saito, N. Takahashi, A. Yokoyama, T. Miyauchi, S. Mori, D. Yano, T. Hakoda, K. Takamiya, K. Nakanishi et al., J. Nucl. Sci. Technol. **34**, 871 (1997)
[20] B.D. Wilkins, E.P. Steinberg, R.R. Chasman, Phys. Rev. C Nucl. Phys. **14**, 1832 (1976)
[21] N. Carjan, F.A. Ivanyuk, Y. Oganessian, G. Ter-Akopian, Nucl. Phys. A **942**, 97 (2015)
[22] Y. Aritomo, S. Chiba, F. Ivanyuk, Phys. Rev. C Nucl. Phys. **90**, 054609 (2014)
[23] Y. Miyamoto, Y. Aritomo, S. Tanaka, K. Hirose, K. Nishio, Phys. Rev. C Nucl. Phys. **99** (2019)
[24] J. Maruhn, W. Greiner, Zeitschrift für Physik **251**, 431 (1972)
[25] H.J. Krappe, J.R. Nix, A.J. Sierk, Phys. Rev. C Nucl. Phys. **20**, 992 (1979)
[26] S.G. Nilsson, C.F. Tsang, A. Sobiczewski, Z. Szymański, S. Wycech, C. Gustafson, I.L. Lamm, P. Möller, B. Nilsson, Nucl. Phys. A **131**, 1 (1969)
[27] A.V. Ignatyuk, G.N. Smirenkin, A.S. Tishin, Yadernaya Fizika **21**, 485 (1975)

[28] Y. Aritomo, M. Ohta, Nucl. Phys. A **744**, 3 (2004)
[29] K.T.R. Davies, A.J. Sierk, J.R. Nix, Phys. Rev. C Nucl. Phys. **13**, 2385 (1976)
[30] A.J. Sierk, J.R. Nix, Phys. Rev. C Nucl. Phys. **21**, 982 (1980)
[31] P. Möller, A.J. Sierk, T. Ichikawa, H. Sagawa, At. Data Nucl. Data Tables **109-110**, 1 (2016)